Article:
Saha, S, Yang, XB orcid.org/0000-0002-0144-2826, Wijayathunga, N et al. (4 more authors) (2019) A biomimetic self-assembling peptide promotes bone regeneration in vivo: A rat cranial defect study. Bone, 127. pp. 602-611. ISSN 8756-3282

https://doi.org/10.1016/j.bone.2019.06.020

TITLE: A biomimetic self-assembling peptide promotes bone regeneration in vivo: a rat cranial defect study

AUTHORS: Sushmita Saha[a], Xuebin B Yang[a], Nagitha Wijayathunga[b], Sarah Harris[c], Georg A Feichtinger[a], R Philip W Davies[a]*, Jennifer Kirkham[a]

[a]Department of Oral Biology, School of Dentistry, St James's University Hospital, University of Leeds, Leeds, UK

[b]School of Mechanical Engineering, University of Leeds, Leeds, UK

[c]School of Physics and Astronomy and Astbury Centre for Structural and Molecular Biology, University of Leeds, Leeds, UK

*Correspondence to:

Dr RPW Davies,
Department of Oral Biology,
School of Dentistry,
Faculty of Medicine & Health
Level 7, Wellcome Trust Brenner Building,
University Of Leeds
St James's University Hospital
Leeds, LS9 7TF
UK

Email:R.P.W.Davies@leeds.ac.uk

Abbreviations: Self assembling peptide(s): SAP(s); Human dental pulp stromal cells: DDPSCs; Bone marrow mesenchymal stem cells: BMMSCs; BMD: Bone mineral density; BV: Bone volume; TV: total volume; Peptide nanofibers: PNF

ABSTRACT

Rationally designed, pH sensitive self-assembling β-peptides (SAPs) which are capable of reversibly switching between fluid and gel phases in response to environmental triggers are potentially useful injectable scaffolds for skeletal tissue engineering applications. SAP P_{11}-4 ($CH_3COQQRFEWEFEQQNH_2$) has been shown to nucleate hydroxyapatite mineral de novo and has been used in dental enamel regeneration. We hypothesised that addition of mesenchymal stromal cells (MSCs) would enhance the in vivo effects of P_{11}-4 in promoting skeletal tissue repair. Cranial defects were created in athymic rats and filled with either Bio-Oss® (anorganic bone chips) or P_{11}-4 ± human dental pulp stromal cells (HDPSCs). Unfilled defects served as controls. After 4 weeks, only those defects filled with P_{11}-4 alone showed significantly increased bone regeneration (almost complete healing), compared to unfilled control defects, as judged using quantitative micro-CT, histology and immunohistochemistry. In silico modelling indicated that fibril formation may be essential for any mineral nucleation activity. Taken together, these data suggest that self-assembling peptides are a suitable scaffold for regeneration of bone tissue in a one step, cell-free therapeutic approach.

Keywords: Self-assembly, Hydrogels, Bone Regeneration, Mesenchymal stromal cells, Calvaria

1. INTRODUCTION

There is a major clinical need to replace bone following loss of tissue due to disease (congenital/genetic), ageing or trauma. Autologous bone grafts possess a histocompatibility advantage and are thus the current gold standard for bone replacement. This procedure does however include serious limitations, such as donor site morbidity, limited tissue supply, temporary loss of function and surgical/anaesthetic risks, [1] prompting the development of novel approaches to bone repair based upon tissue regeneration. These have been based upon the use of (either alone or in combinations) adult mesenchymal stem cells [2,3], synthetic/natural scaffolds or cytokines, with the ultimate aim of promoting a tissue rich in collagens and mineral within bone defects [2,4–8]. Biomaterials with hydroxyapatite coatings [9] or materials where all the organic component of allogenic bone has been removed, leaving behind the apatitic mineral phase e.g. Bio-Oss® (Geistlich, Switzerland), OsteoGraf/N (Dentsply, Germany) have proven success in restoring lost bone but can be disadvantaged by their relatively long degradation rates [10]. Bio-Oss® has been reported to be resorbed by osteoclast-like cells in vivo but remnants of the biomaterial have been observed several years post implantation in some patients [11–13]. An ideal biomaterial for bone regeneration should not only provide biocompatibility, appropriate porosity and osteo-conduction/induction but should also possess a biodegradation rate broadly corresponding to that of new bone formation [14].

A range of designer self-assembling peptides (SAPs) are being investigated by various groups for their potential use as scaffolds in regenerative medicine. The ability of SAPs to self-assemble when triggered by environmental cues and their potential to modulate certain parameters such as cell adhesion, mechanical stiffness and biodegradation by varying the peptide sequence makes them an attractive biomaterial for cell-based tissue repair [15].

Aggeli and colleagues designed a family of 11^{-mer} peptides (with varying overall charge, hydrophobicity and polarity) that self-assemble in response to different physico-chemical triggers to produce hydrogels at peptide concentrations of 10-30 mg/mL [16]. P_{11}-4 (primary sequence $CH_3COQQRFEWEFEQQNH_2$) is one such SAP with an overall net charge of -2 at physiological pH, that undergoes pH triggered self-assembly to form a self-supporting hydrogel in a concentration dependent manner [17–19]. P_{11}-4 has shown promise as an injectable scaffold for hard tissue engineering applications including its use as an injectable lubricant for osteoarthritis and is already in clinical use as a regenerative treatment for early dental decay (caries) based upon its proven ability to nucleate hydroxyapatite mineral de novo [17,20–22]. Furthermore, P_{11}-4 has a distinct physical advantage over other scaffolds such that when it is shear softened, P_{11}-4 will return to its original gel state, without phase separating [19], offering a capable encapsulating delivery and biomimetic scaffold.

A synergistic combination of an appropriate biomaterial with a suitable cell source is believed to result in regenerated tissue with a biochemical and mechanical composition similar to that of the native tissue [23]. Owing to their intrinsic properties (self-renewal and immunomodulatory), stem cells are a favoured cell source for use in bone tissue regeneration. Whilst bone marrow mesenchymal stem cells (BMMSCs) extracted from the iliac crest remain the best understood and most studied stem cell source used in bone tissue engineering [24,25], human dental pulp stromal cells (HDPSCs) have also been the subject of much investigation since they were first described by Gronthos et al (2000). They have since been shown to have multiple lineage potential and express many of the cell surface markers used to characterise bone marrow derived MSCs (new REFS). HDPSCs can be easily obtained without any invasive surgery by banking deciduous (“milk”) teeth (“SHED”) [26]. In addition, these cells are documented to possess a higher proliferation rate and enhanced osteogenic differentiation potential when compared to human bone marrow stromal cells

(HBMSCs) [27,28]. A combination of these properties makes HDPSCs an attractive cell source for bone tissue engineering.

The aim of this study was to test the hypothesis that HDPSCs used in conjunction with P_{11}-4 hydrogels would enhance regeneration of bone in vivo in a rat calvaria defect model. Our underlying hypothesis was that P_{11}-4's known ability to nucleate hydroxyapatite[20], coupled with the potential of HDPSCs to provide instructional cues to resident cells and their pro-mineralising characteristics, would accelerate bone repair over and above the use of the P_{11}-4 alone.

2. MATERIALS & METHODS:

2.1 SAP Synthesis

Self-assembling peptide P_{11}-4 is monomeric at high pH and low salt concentration and forms fibrils at low pH and physiological salt concentrations. The peptides used in this study were custom synthesised by CS Bio Co., California and were shown to be greater than 95% (w/w) pure using HPLC analysis. The peptide was sterilized in the dry state using a Gammacell irradiator.

2.2. L929 Cell culture

L929 cells used for biocompatibility testing experiments were obtained from Sigma Aldrich (UK) and maintained in DMEM with 2 mM glutamine, 10% fetal calf serum (FCS) including 10,000 units penicillin and 10 mg streptomycin/mL. Semi-confluent cultures were split 1:4 to 1:6 i.e. seeding at 2 $x10^4$ cells /cm^2 using 0.25% trypsin and cultured in an incubator set at 5% CO_2; 37°C.

2.3. P_{11}-4 Biocompatibility testing

Biocompatability testing was carried out in accordance with international standard ISO 10993-5-2009 using the well defined murine fibroblast cell line L929.

For the extract test, P_{11}-4 peptides were dissolved (10 mg/mL; 6.27 mM) in DMEM supplemented with antibiotics, L-glutamine and 10% fetal calf serum (DMEM/ 10% FCS). The peptides were monomerised by transient exposure to alkaline pH (pH 8.4; 30 minutes) and then gelled by acidification (pH 7.4). The resulting gels were incubated at 37°C for 24 hours, centrifuged (2000 rpm; 5 min) and the supernatants (termed 'P_{11}-4 extracts') collected. The medium was removed from cultures of L929 cells ($1x10^4$ cells/well in 96 well plates) and the cells treated with 100 µL of either (i) undiluted P_{11}-4 extract, (ii) P_{11}-4 extract diluted with DMEM/ 10% FCS (80, 60, 40, 20 and 10% final concentration), (iii) DMEM/ 10% FCS supplemented with 10% PBS, (iv) DMEM/ 10% FCS only (positive control) or (v) DMEM/ 10% FCS containing phenol (6.4 mg/mL; negative control) for 24 hours at 37ºC in a humidified atmosphere of 5% CO_2. MTT (3-(4,5-dimethylthiazol-2-yl)-2,5-diphenyl tetrazolium bromide solution; 1 mg/mL in DMEM/ 10% FCS; 50µL) was then added to each of the wells and the cultures incubated for a further 2 hours. The fluid within the wells was aspirated and isopropanol (100 µL) added to each. The samples were placed on an orbital shaker until all the crystals had dissolved and the absorbance of the resulting solutions measured using a plate reader (OD570-OD650). Results were expressed as a percentage of the positive control.

For direct contact cytotoxicity testing**,** P_{11}-4 (30 mg/mL in DMEM/ 10% FCS; 20 µL) was added to the wells of a 24 well plate and the material allowed to gel and adhere for 2 hours. L929 cells ($2x\ 10^5$ cells in 700 µL of DMEM/10% FCS) were then added to each well and the cultures observed periodically for 48 hours. The cultures were then treated with MTT (1 mg/mL as above) for a further 2 hours and imaged by digital microscopy.

2.4 Human dental pulp stem cell isolation and culture

Third molar ("wisdom") teeth were obtained through the Leeds Skeletal Tissues Research Tissue Bank (National Research Ethics Service Research Ethics Committee of Leeds East:

07/H1306/95+5) from patients attending the Leeds Dental Institute with full patient consent and ethical approval (Dentistry Research Ethics Committee No. 210311/SS/62). Cells were isolated using the collagenase digestion method previously described by Ricordi et al. (1992) and Gronthos et al. (2000) [29,30]. The isolated HDPSCs were maintained in α-MEM medium supplemented with 10% FBS (Lonza), 2 mM L-glutamine (Sigma), 10,000 units penicillin and 10 mg streptomycin/mL (Sigma) at 37°C and 5% CO_2 until 80% confluent. Passage 4 cells (P4) were used in this study.

2.5 Preparation of SAP-cell hydrogels and Bio-Oss® for in vivo implantation

HDPSCs (P4) were trypsinised and 5×10^4 cells were suspended in 1 mL of phosphate buffered saline (PBS) to which 30 mg of sterile P_{11}-4 were added. The pH was adjusted to 7.4 with 0.5 M hydrochloric acid and the P_{11}-4-cell construct was thoroughly mixed by pipetting before being allowed to self-assemble in a 1 mL sterile syringe barrel. Capped sterile needles were fixed onto the syringes in order to maintain sterility. P_{11}-4 containing no cells but assembled as described above was used as a control. Bio-Oss® granules of 0.25-1 mm size were gamma sterilised and used as a positive control.

2.6 In vivo implantation in rat calvaria defect model

All in vivo studies were carried out under UK Home Office Project License approval. Adult athymic male rats (Hsd: RH-Foxn1^{rnu}) were obtained from Harlan Laboratories, Netherlands. Animals were anesthetised using 4% isoflurane in oxygen and anaesthesia was maintained with 2% isoflurane in oxygen. Any fine hairs present between the bridge of the snout between the eyes to the caudal end of the calvarium were shaved using electric clippers followed by use of an alcohol swab to sterilise the skin surface. An incision down to the periosteum was made along the mid-sagittal crest of the calvarium to expose the bone beneath. Clear visibility of the line of sagittal suture of the calvarial bone helped to divide the skull into two halves. A 4 mm diameter circular defect was created in each half of the skull using a trephine

burr under profuse sterile saline irrigation. Special care was taken to leave the underlying dura mater undamaged. Sterile Bio-Oss® granules were placed into the defect using a sterile spatula and patted down until the defect was fully covered with the particles. P_{11}-4 (with or without cells) assembled in sterile syringes was injected into the defect and patted down using a sterile spatula to fully cover the defect. Control defects were left empty. After filling the defect with the appropriate material according to the experimental group (Table 1), the surgical site was covered by suturing the periosteum followed by suturing of the skin. Post-operative analgesia was administered and following observations of purposeful movement, the animals were transferred to their cages.

Table 1

2.7 Specimen preparation and micro-computed tomography (micro-CT) analysis

Animals from each group were sacrificed at 4 or 6 weeks post-surgery. The calvarial bone was dissected and removed and immediately fixed in 10% neutral buffered formalin. Micro-computed tomography (micro-CT) scanning was carried out using a microCT-100, (Scanco Medical AG, Switzerland) consisting of a cone-beam x-ray source and fitted with a 0.5 mm aluminium filter. The rat calvaria samples were each placed in a sample holder along with two rat bone phantoms (Bruker, Belgium). The hydroxyapatite (HA) densities of the phantoms were 0.25 gHA/cm^3 and 0.75 g HA/cm^3 respectively. The hydroxyapatite (HA) densities of the phantoms were 0.25 gHA/cm^3 and 0.75 g HA/cm^3 respectively. The scanner settings were: voltage 70 kVp, current 114 mA, integration time 300 ms, in combination with 10 μm nominal resolution, 3522 x 3522 customised matrix size and a beam hardening correction algorithm based on a HA-phantom (1.200 g HA/cm^3) provided by the CT manufacture .

Analysis of scans was conducted on volumes of interest. In all cases a Gaussian filter (sigma =0.8, support =1.0) was applied to minimize high frequency noise. Greyscale thresholding was conducted by an experienced CT user working blind and the best fit was obtained considering the entire stack rather than a single slice. The Bone Mineral Density (BMD) and the ratio of Bone Volume to Total Volume (BV/TV) were obtained from the thresholded image stacks using algorithms provided by the manufacturer. The density values derived from the scans for the rat phantoms were 0.259 and 0.758 g HA/cm^3 respectively, indicating that the scanner density calibration was accurate for the intended analysis.

2.8 Statistical Analysis

Statistical analysis of regenerated/total bone volume and regenerated bone mineral density values was performed using the Kruskal Wallis non-parametric test with Dunns post-test, using GraphPad Prism Software (GraphPad Software, Inc., San Diego, CA, USA).

2.9 Histological analysis

Following micro-CT analysis, the fixed calvaria were first demineralised in 14% EDTA for four weeks. Following confirmation of demineralisation via X-ray imaging, the calvaria samples were embedded in paraffin wax and 5 µm thick serial sections were prepared coronally to the defect using a microtome (Leica). The sections were stained with Van Gieson stain. Stained sections were imaged under a Zeiss, Axio Imager M2 microscope and analysed using Zen Pro software (Ver. 2012).

2.10 Immunohistochemical analysis

Immunohistochemical analysis was performed on 5 µm thick formalin-fixed paraffin sections. Endogenous peroxidase activity was blocked using 2% hydrogen peroxide and chymotrypsin (Sigma) enzymatic antigen retrieval was carried out by incubating sections in a 0.1% enzyme solution (pH 7.8) for 30 minutes. Samples were incubated overnight at 4°C with specific primary antibodies against type I collagen (mouse monoclonal anti-collagen I;

1:300; Abcam), and osteocalcin (mouse monoclonal anti-osteocalcin; 1:100; Abcam) and staining was achieved using peroxidase conjugated secondary antibodies as per the manufacturer's protocol (EnVision Kit, Dako). Nuclei were counterstained with haematoxylin. The stained sections were visualized using an Olympus BX50 microscope and imaged using NIS Elements BR software (Ver. 3.0).

2.11 In silico modelling

Atomistic molecular dynamics (MD) simulations were performed using the AMBER11 suite of programs in conjunction with the AMBER99SB forcefield [31,32]. Fibril models were constructed using the Nucleic Acid Builder (NAB) software package [33], then calcium ions and sufficient TIP3P water molecules were added to ensure a solvent layer of at least 10Å in each orthogonal direction. The locations of the calcium ions were randomised to ensure that all of the ions were located at least 3Å away from the surface of the peptide tape prior to MD. All calculations employed periodic boundary conditions and used the Ewald summation technique in the PMEMD module of AMBER11 to correctly account for long range electrostatic interactions. Prior to the MD production runs, the tapes were energy minimised and equilibrated as previously described [34]. Calcium ion-surface interactions were established over short (within 500 ps) MD simulation trajectory timescales.

3. RESULTS

3.1 Biocompatibility testing

Using the MTT assay showed that P_{11}-4 gel extracts had no statistically significant adverse effects upon L929 cell viability (Figure 1A), suggesting that the P_{11}-4 gel had released no soluble cytotoxic molecules/material. By comparison, the phenol control produced a complete loss of cell viability. Viable L929 cells were observed growing directly in contact with the peptide in the contact cytotoxicity testing (Figure 1B).

Figure 1

3.2 Micro CT analysis: Bone volume and bone mineral density

Macroscopically, in samples where defects were filled with P_{11}-4, it was difficult to distinguish new bone from surrounding native tissue in retrieved defects whereas Bio-Oss® particles could be clearly distinguished from the surrounding native calvaria bone. To evaluate new bone formation, 3D micro-CT scans were obtained at 4 and 6 weeks post surgery. Reconstructed 3D micro-CT scans showed a clear circular demarcation where the defect had been created making it easier to determine the volume of any newly regenerated bone (typical reconstructions are shown in Figure 2). The reconstructed images showed that the control (unfilled) defects remained unrepaired during the time of the experiment and that filling the defects with P_{11}-4 ± cells had resulted in deposition of mineralised tissue at both time points, with complete healing observed in some cases. There was a clear trend for P_{11}-4 alone to have higher proportions of regenerated bone in the defect than P_{11}-4 with cells. Three out of 6 defects filled with P_{11}-4 alone showed almost complete healing at 4 weeks. In contrast, 0 out of 6 defects filled with P_{11}-4 including cells showed thoroughly mineralised areas in the defects (Figure 2; D-F). Defects filled with Bio-Oss® appeared dense in the CT micrographs at 4 weeks (Figure 2; A-C) as would be expected given that these are particles of anorganic bone. However, at 6 weeks, CT micrographs of samples where defects had been filled with Bio-Oss® revealed examples of non-mineralised/very low density regions, possibly indicating resorbtion of the Bio-Oss® in these cases.

Quantitative assessment of total bone volume (TBV) within the defects after 4 weeks showed a significantly higher amount of mineralised tissue where P_{11}-4 alone had been used compared with the empty defect controls (Figure 3A). No statistically significant differences

were found between the groups at 6 weeks, however, 3 out of 6 defects filled with P_{11}-4+cells and 4 out of 6 defects filled with P_{11}-4 alone showed almost complete healing of the defect. The greater variability of TBV in the case of defects filled with Bio-Oss® compared with the much smaller variability in TBV for defects filled with P_{11}-4 ± cells supported the observation that Bio-Oss® resorption may have taken place at this later time point (Figure 3B). There was no significant difference in bone mineral density for any of the groups at either time point. Bone mineral density values measured were similar to that of native rat calvaria bone (Figure 4).

Figure 3

Figure 4

3.3 Histological observations

After 4 weeks, samples where the defects were filled with Bio-Oss® revealed small islands of new bone growth near the defect margins. The Bio-Oss® stained light blue and was visible as small granules (Figure 5A, marked with an asterix). The unfilled control defects showed a similar pattern of new bone formation with small areas of bone growth at the defect margins (Figure 5B). Samples where the defects where filled with the P_{11}-4 alone showed extensive new bone formation at 4 weeks and in some samples the defect margins were almost indistinguishable from the newly regenerated bone (Figure 5 C). Van Gieson stain for these samples also detected collagen (blue colour) in the regenerated bone distributed similarly to that observed in native rat calvaria. Samples where defects were filled with P_{11}-4 combined with HDPSCs also showed extensive new bone formation (apparently arising from marginal infilling); however non-mineralised areas within the defect were more prominent compared

to those filled with P_{11}-4 alone. The outer extent of new bone formed in these two groups was slightly less than that of the surrounding calvarial bone (Figure 5, C-D).

After 6 weeks, fewer Bio-Oss® granules were detected in the filled defects, further suggesting resorption of the particles with time (Figure 5 E) whilst slightly more extensive new bone formation was observed in the unfilled control samples compared with their 4 week counterparts. Defects filled with P_{11}-4 ± cells showed extensive new bone formation after 6 weeks (Figure 5 G-H). In these defects, staining for collagen and the outer extent of new bone formation almost matched that of the surrounding native bone (Figure 6).

Figure 5

3.4 Immunohistolocalisation of osteocalcin and type 1 collagen

Immunohistochemical analysis was carried out to determine the extent of the presence of osteocalcin and collagen type I in the matrix of any newly regenerated bone in each experimental group. Defects filled with Bio-Oss® and unfilled controls showed faint osteocalcin staining, indicating, a lack of extensive mature new bone formation in these samples (Figure 6A-B, E-F). For defects filled with P_{11}-4 ± HDPSCs, immunohistochemical staining for osteocalcin at both 4 and 6 weeks revealed similar high staining intensities within the newly regenerated bone (Figure 6C-D, G-H) and the surrounding native bone.

Collagen type I was not detected in unfilled control defects at either of the time points (Figure 7B-F) whilst faint staining only was observed interspersed between the Bio-Oss® granules at week 4 (Figure 7A). Intense immunohistochemical staining for collagen type I was detected in new bone formed in defects filled with P_{11}-4 ± HDPSCs after both 4 (Figure 7C-D) and 6 weeks. The intensity of staining resembled that seen in the surrounding native calvarial bone.

Figure 6

Figure 7

3.5 In silico modelling of P_{11}-4 – calcium interactions

The predicted behaviour of P_{11}-4 under conditions of physiological pH and ionic strength is shown in Figure 8. Computer modelling using AMBER software predicted that P_{11}-4 in its assembled form presents an array of potential binding sites for calcium ions. Figure 8B shows an image of a computer model of a ribbon of P_{11}-4 comprising of 32 individual P_{11}-4 monomers arranged anti-parallel and 48 ions of calcium. Calcium ions were observed to preferentially dock between the side chains of four adjacent glutamate (E) residues (negatively charged at pH 7.4) in the molecular dynamics simulations, as shown in Figure 8B. Little calcium binding was predicted in association with glutamate residues at position 9 in the primary sequence and almost no other calcium binding was seen elsewhere. Little calcium binding was predicted in association with glutamate residues at position 9 in the primary sequence and almost no other calcium binding was seen elsewhere.

Figure 8

4. DISCUSSION

Self-assembling peptides potentially offer advantages over other biomaterials for use in skeletal tissue repair: bulk chemical synthesis ensures economies of scale and higher reproducibility; they have a long shelf life; are free from zoonoses; can be easily and effectively functionalised and can serve to mimic 3D extracellular matrices [23]. The transition from monomeric to self-assembled states of P_{11}-4 can be manipulated according to the environmental conditions required. P_{11}-4 has the ability to form hydrogels as a direct result of the hierarchical self-assembly of chiral rod like units (anti-parallel beta sheet tapes

stacked to form ribbons which in turn stack to form fibrils and finally fibres) above a critical gelation concentration (>10 mg/mL) at neutral pH [19,35]. The advantages of being able to reversibly control the self-assembly process by adjusting the pH of the solvent along with this peptide's biocompatibility, biodegradability, injectability, positive reaction to shear softening and ability to nucleate hydroxyapatite de novo make P_{11}-4 an attractive scaffold for possible use in bone tissue engineering [18]. In a previous study, three P_{11}-series SAPs were screened for their ability to promote bone repair in a rabbit calvarial model [36] confirming their ability to promote skeletal tissue regeneration and repair.

In the present study, we hypothesised that the addition of exogenous MSCs to SAPs might accelerate the previously observed bone regeneration process by stimulating osteogenesis. We selected P_{11}-4 as the candidate scaffold for use in our experiments as this peptide is not only already licensed for clinical use in Dentistry but also has assembly characteristics that are directly compatible with use as a scaffold in vivo. We elected to combine P_{11}-4 with HDPSCs to test our hypothesis as these cells have been repeatedly reported to favour a mineralised tissue phenotype [37] and have been shown to have the capacity for regeneration of bone in vivo (New refs). We would therefore not expect any differences in outcome of our experiments to be related to HDPSCs lack of potential for osteodifferentiation.

We used skeletally mature rats with an average weight of 280 g (14 weeks old) as bone defects in young/skeletally immature rodents are known to heal spontaneously [38]. The unfilled control defects failed to heal within our 6 week observational time point and as such permitted comparison with our experimental treatments. Whilst in this study a statistical significance between total regenerated bone volume in P_{11}-4 alone samples compared to P_{11}-4+ MSCs wasn't observed, overall higher bone regeneration was observed in P_{11}-4 alone samples at 4 weeks. By 6 weeks, P_{11}-4 + cells samples showed similar bone repair compared to P_{11}-4 alone and the Bio-Oss® group. Defects filled with P_{11}-4 (alone or with MSCs)

revealed histological findings with similar distribution and staining intensities of the osteogenic markers collagen type I and osteocalcin in the neo-tissue formed in the defect compared to the surrounding natural calvarial bone.

Our data indicated that filling the calvarial defects with P_{11}-4 alone (without cells) appeared to accelerate the healing process at week 4 compared with unfilled control defects. Given that both treatments (P_{11}-4 ± cells) . generated similar amounts of new bone by week 6, our hypothesis that the addition of MSCs (at least in the form of HDPSCs) would accelerate bone repair, is rejected. Our findings support those of other researchers who showed that $(KLDL)_{3,}$ a self-assembling peptide capable of stimulating chondrogenesis of BMMSCs in vitro produced significantly higher osteochondral regeneration in vivo when used without any additional cells compared to the results obtained when the SAP was delivered in combination with BMMSCs [39].

We did not track the fate of the HDPSCs that we used in our experiments in vivo but there are reports that demonstrate persistent engraftment of adult human MSCs when transplanted into immunoincompetent/ athymic xenogenic models (rats) [40,41]. We thus assume that our MSCs transplanted into the athymic rat calvarias survived the initial transplantation and engrafted within the defect. It is, however, known that MSCs rapidly lose 'stemness' (multipotential differentiation ability) and their homing ability when they are first cultured in vitro [42]. This could be a possible explanation as to why our P_{11}-4/HDSPC constructs failed to outperform/augment bone repair compared to P_{11}-4 alone. Alternatively, it is possible that the SAP gel poses a barrier to free diffusion of the necessary cues to induce osteogenesis in the HDSPCs.

Biomaterials used as scaffolds for skeletal tissue repair need to provide transient support i.e. the materials' degradation kinetics must match that of the rate of new tissue formation [43]. Self-assembling peptides can be enzymatically degraded via hydrolysis of the amide bonds

between their constituent amino acids by endogenous peptidases [44,45]. Mazza and colleagues (2013) observed that peptide nanofibres (PNFs) that underwent self-assembly were structurally unstable in biological medium that contained enzymes. The peptidases disassociated the PNFs into smaller fragments before structural degradation during enzyme-mediated disassembly[45]. SAPs mixed with cells are therefore more likely to degrade faster than SAPs alone as they are subjected not only to endogenous in vivo peptidase activity but also to enzymatic degradation by the additional ex-vivo cells. In our experiments, P_{11}-4 alone perhaps degraded at a slower rate that is more suitable to support osteogenesis and bone remodelling compared to P_{11}-4 combined with HDPSCs, which would explain why we see enhanced bone volume in defects filled with P_{11}-4 only. Our in silico modelling data suggested that (assembled) P_{11}-4 fibrils are capable of nucleating hydroxyapatite mineral via negatively charged domains attracting calcium ions with consequential formation of a critical nucleus for hydroxyapatite formation under physiological conditions. This ability of P_{11}-4 to act as a heterogeneous nucleator in the assembled form would be lost if the fibrils were to be quickly degraded.

5. CONCLUSION

In this study we have demonstrated accelerated healing of calvarial defects as seen by cumulative total bone volume and bone mineral density values, Van Gieson histological staining and osteocalcin and collagen type I immunostaining. This repair was not enhanced by the addition of HDPSCs. Mechanistic factors (including those dictating the micro-environment within the hydrogels) influencing bone repair associated with self-assembling peptides remain to be elucidated, as, indeed, does the fate of the engrafted cells themselves.However, taken overall, the data presented here suggest that the self-assembling

peptide P_{11}-4, in its assembled state, appears to offer a suitable candidate material for bone tissue engineering.

Acknowledgements

This work was supported by WELMEC, a Centre of Excellence in Medical Engineering funded by the Wellcome Trust and EPSRC, under grant number WT 088908/Z/09/Z; JK and XY are supported by NIHR through the Leeds Musculoskeletal Biomedical Research Unit. We thank Dr Amalia Aggeli (Aristotle University of Thessaloniki, Greece), for her advice and input in to the use of self assembling peptides during this project.

Conflicts of interest:

JK is a named co-inventor of the use of self assembling peptides, including P_{11}-4, as scaffolds for tissue engineering. There are no other conflicts of interest.

Figure Legends

6. REFERENCES

[1] E.M. Younger, M.W. Chapman, Morbidity at bone graft donor sites., J. Orthop. Trauma. 3 (1989) 192–195. doi:10.1097/00005131-198909000-00002.

[2] N. Wada, S. Gronthos, P.M. Bartold, Immunomodulatory effects of stem cells, Periodontol. 2000. 63 (2013) 198–216.

[3] J.R. Mauney, V. Volloch, D.L. Kaplan, Role of adult mesenchymal stem cells in bone tissue engineering applications: current status and future prospects, Tissue Eng. 11 (2005) 787–802.

[4] J.S. Lee, S.D. Baek, J. Venkatesan, I. Bhatnagar, H.K. Chang, H.T. Kim, S.-K. Kim, In

vivo study of chitosan-natural nano hydroxyapatite scaffolds for bone tissue regeneration, Int. J. Biol. Macromol. 67 (2014) 360–366.

[5] J. Wang, H. Yan, T. Chen, Y. Wang, H. Li, W. Zhi, B. Feng, J. Weng, M. Zhu, Porous nanoapatite scaffolds synthesized using an approach of interfacial mineralization reaction and their bioactivity, J. Biomed. Mater. Res. Part B Appl. Biomater. 102 (2014) 1749–1761.

[6] J. Hu, Y. Zhou, L. Huang, J. Liu, H. Lu, Effect of nano-hydroxyapatite coating on the osteoinductivity of porous biphasic calcium phosphate ceramics, BMC Musculoskelet. Disord. 15 (2014) 114.

[7] T. Long, Y. Liu, S. Tang, J. Sun, Y. Guo, Z. Zhu, Hydrothermal fabrication of hydroxyapatite/chitosan/carbon porous scaffolds for bone tissue engineering, J. Biomed. Mater. Res. Part B Appl. Biomater. 102 (2014) 1740–1748.

[8] X. Huang, X. Liu, S. Liu, A. Zhang, Q. Lu, D.L. Kaplan, H. Zhu, Biomineralization regulation by nano-sized features in silk fibroin proteins: Synthesis of water-dispersible nano-hydroxyapatite, J. Biomed. Mater. Res. Part B Appl. Biomater. 102 (2014) 1720–1729.

[9] C. Du, F.Z. Cui, X.D. Zhu, K. de Groot, Three-dimensional nano-HAp/collagen matrix loading with osteogenic cells in organ culture, J. Biomed. Mater. Res. 44 (1999) 407–415.

[10] N. Tovar, R. Jimbo, R. Gangolli, L. Perez, L. Manne, D. Yoo, F. Lorenzoni, L. Witek, P.G. Coelho, Evaluation of bone response to various anorganic bovine bone xenografts: an experimental calvaria defect study, Int. J. Oral Maxillofac. Surg. 43 (2014) 251–260.

[11] M. Duda, J. Pajak, The issue of bioresorption of the Bio-Oss xenogeneic bone

substitute in bone defects., in: Ann. Univ. Mariae Curie. Sklodowska. Med., 2003: pp. 269–277.

[12] M.A.W. Merkx, J.C. Maltha, M. Van't Hoff, A.-M. Kuijpers-Jagtman, H.-P. Freihofer, Tooth eruption through autogenous and xenogenous bone transplants: a histological and radiographic evaluation in beagle dogs, J. Cranio-Maxillofacial Surg. 25 (1997) 212–219.

[13] D. Zaffe, G.C. Leghissa, J. Pradelli, A.R. Botticelli, Histological study on sinus lift grafting by Fisiograft and Bio-Oss, J. Mater. Sci. Mater. Med. 16 (2005) 789–793.

[14] R. Langer, J. Vacanti, Tissue engineering, Science (80-.). 260 (1993) 920–926. doi:10.1126/science.8493529.

[15] P.W. Kopesky, E.J. Vanderploeg, J.S. Sandy, B. Kurz, A.J. Grodzinsky, Self-assembling peptide hydrogels modulate in vitro chondrogenesis of bovine bone marrow stromal cells, Tissue Eng. Part A. 16 (2009) 465–477.

[16] A. Aggeli, I.A. Nyrkova, M. Bell, R. Harding, L. Carrick, T.C.B. McLeish, A.N. Semenov, N. Boden, Hierarchical self-assembly of chiral rod-like molecules as a model for peptide beta-sheet tapes, ribbons, fibrils, and fibers, Proc. Natl. Acad. Sci. U. S. A. 98 (2001) 11857–11862. doi:10.1073/pnas.191250198.

[17] C.J. Bell, L.M. Carrick, J. Katta, Z. Jin, E. Ingham, A. Aggeli, N. Boden, T.A. Waigh, J. Fisher, Self-assembling peptides as injectable lubricants for osteoarthritis, J. Biomed. Mater. Res. Part A. 78 (2006) 236–246.

[18] S. Kyle, A. Aggeli, E. Ingham, M.J. McPherson, Recombinant self-assembling peptides as biomaterials for tissue engineering, Biomaterials. 31 (2010) 9395–9405. doi:10.1016/j.biomaterials.2010.08.051.

[19] L.M. Carrick, A. Aggeli, N. Boden, J. Fisher, E. Ingham, T. a. Waigh, Effect of ionic

strength on the self-assembly, morphology and gelation of pH responsive ??-sheet tape-forming peptides, Tetrahedron. 63 (2007) 7457–7467. doi:10.1016/j.tet.2007.05.036.

[20] J. Kirkham, A. Firth, D. Vernals, N. Boden, C. Robinson, R.C. Shore, S.J. Brookes, A. Aggeli, Self-assembling peptide scaffolds promote enamel remineralization, J. Dent. Res. 86 (2007) 426–430.

[21] A. Firth, A. Aggeli, J.L. Burke, X. Yang, J. Kirkham, Biomimetic self-assembling peptides as injectable scaffolds for hard tissue engineering, (2006).

[22] P.A. Brunton, R.P.W. Davies, J.L. Burke, A. Smith, A. Aggeli, S.J. Brookes, J. Kirkham, Treatment of early caries lesions using biomimetic self-assembling peptides–a clinical safety trial, Br. Dent. J. 215 (2013) E6–E6.

[23] A. Horii, X. Wang, F. Gelain, S. Zhang, Biological designer self-assembling peptide nanofiber scaffolds significantly enhance osteoblast proliferation, differentiation and 3-D migration, PLoS One. 2 (2007) e190.

[24] P. Bianco, P. Gehron Robey, Marrow stromal stem cells, J. Clin. Invest. 105 (2000) 1663–1668. doi:10.1172/JCI10413.

[25] D. Kaigler, G. Pagni, C.H. Park, T.M. Braun, L.A. Holman, E. Yi, S.A. Tarle, R.L. Bartel, W. V Giannobile, Stem cell therapy for craniofacial bone regeneration: a randomized, controlled feasibility trial, Cell Transplant. 22 (2013) 767.

[26] Y. Yamada, S. Nakamura, K. Ito, T. Sugito, R. Yoshimi, T. Nagasaka, M. Ueda, A feasibility of useful cell-based therapy by bone regeneration with deciduous tooth stem cells, dental pulp stem cells, or bone-marrow-derived mesenchymal stem cells for clinical study using tissue engineering technology, Tissue Eng. Part A. 16 (2010) 1891–1900.

[27] D.L. Alge, D. Zhou, L.L. Adams, B.K. Wyss, M.D. Shadday, E.J. Woods, G. Chu, W.S. Goebel, Donor-matched comparison of dental pulp stem cells and bone marrow-derived mesenchymal stem cells in a rat model, J. Tissue Eng. Regen. Med. 4 (2010) 73–81.

[28] K. Ito, Y. Yamada, S. Nakamura, M. Ueda, Osteogenic potential of effective bone engineering using dental pulp stem cells, bone marrow stem cells, and periosteal cells for osseointegration of dental implants., Int. J. Oral Maxillofac. Implants. 26 (2011).

[29] C. Ricordi, A.G. Tzakis, P.B. Carroll, Y. Zeng, H.L.R. Rilo, R. Alejandro, R. Shapiro, J.J. Fung, A.J. Demetris, D.H. Mintz, Human islet isolation and allotransplantation in 22 consecutive cases, Transplantation. 53 (1992) 407.

[30] S. Gronthos, M. Mankani, J. Brahim, P.G. Robey, S. Shi, Postnatal human dental pulp stem cells (DPSCs) in vitro and in vivo, Proc. Natl. Acad. Sci. 97 (2000) 13625–13630.

[31] D.A. Case, V. Babin, J.T. Berryman, R.M. Betz, Q. Cai, D.S. Cerutti, T.E.I. Cheatham, T.A. Darden, R.E. Duke, H. Gohlke, A.W. Goetz, S. Gusarov, N. Homeyer, P. Janowski, J. Kaus, I. Kolossváry, A. Kovalenko, T.S. Lee, S. LeGrand, T. Luchko, R. Luo, B. Madej, K.M. Merz, F. Paesani, D.R. Roe, A. Roitberg, C. Sagui, R. Salomon-Ferrer, G. Seabra, C.L. Simmerling, W. Smith, J. Swails, R.C. Walker, J. Wang, R.M. Wolf, X. Wu, P.A. Kollman, Amber 14, (2014).

[32] D.A. Case, T.E. Cheatham, T. Darden, H. Gohlke, R. Luo, K.M. Merz, A. Onufriev, C. Simmerling, B. Wang, R.J. Woods, The Amber biomolecular simulation programs, J. Comput. Chem. 26 (2005) 1668–1688.

[33] T.J. Macke, D.A. Case, Modeling unusual nucleic acid structures, Am. Chem. Soc. (1998) 379–393.

[34] H. Ndlovu, A.E. Ashcroft, S.E. Radford, S.A. Harris, Effect of sequence variation on the mechanical response of amyloid fibrils probed by steered molecular dynamics simulation, Biophys. J. 102 (2012) 587–596.

[35] A. Aggeli, M. Bell, L.M. Carrick, C.W.G. Fishwick, R. Harding, P.J. Mawer, S.E. Radford, A.E. Strong, N. Boden, pH as a trigger of peptide β-sheet self-assembly and reversible switching between nematic and isotropic phases, J. Am. Chem. Soc. 125 (2003) 9619–9628. doi:10.1021/ja021047i.

[36] J.K. Julie L Burke, Amalia Aggeli, Xuebin Yang, Repair of Bone Defects Using Biomimetic Self-Assembled Peptide Scaffolds, J Dent Res. 88 (2009).

[37] R. El-Gendy, X.B. Yang, P.J. Newby, A.R. Boccaccini, J. Kirkham, Osteogenic differentiation of human dental pulp stromal cells on 45S5 Bioglass® based scaffolds in vitro and in vivo, Tissue Eng. Part A. 19 (2012) 707–715.

[38] T.M. Sweeney, L.A. Opperman, J.A. Persing, R.C. Ogle, Repair of critical size rat calvarial defects using extracellular matrix protein gels, J. Neurosurg. 83 (1995) 710–715.

[39] R.E. Miller, A.J. Grodzinsky, E.J. Vanderploeg, C. Lee, D.J. Ferris, M.F. Barrett, J.D. Kisiday, D.D. Frisbie, Effect of self-assembling peptide, chondrogenic factors, and bone marrow-derived stromal cells on osteochondral repair, Osteoarthr. Cartil. 18 (2010) 1608–1619.

[40] K.H. Grinnemo, A. Månsson, G. Dellgren, D. Klingberg, E. Wardell, V. Drvota, C. Tammik, J. Holgersson, O. Ringden, C. Sylven, Xenoreactivity and engraftment of human mesenchymal stem cells transplanted into infarcted rat myocardium, J. Thorac. Cardiovasc. Surg. 127 (2004) 1293–1300.

[41] J.L. Tremoleda, N.S. Khan, V. Mann, S.N. Racey, A.J. Martin, A. Simpson, B.S.

Noble, Assessment of a preclinical model for studying the survival and engraftment of human stem cell derived osteogenic cell populations following orthotopic implantation, J Musculoskelet Neuronal Interact. 12 (2012) 241–253.

[42] S. Morikawa, Y. Mabuchi, Y. Kubota, Y. Nagai, K. Niibe, E. Hiratsu, S. Suzuki, C. Miyauchi-Hara, N. Nagoshi, T. Sunabori, Prospective identification, isolation, and systemic transplantation of multipotent mesenchymal stem cells in murine bone marrow, J. Exp. Med. 206 (2009) 2483–2496.

[43] F. Yang, J. Wang, L. Cao, R. Chen, L. Tang, C. Liu, Injectable and redox-responsive hydrogel with adaptive degradation rate for bone regeneration, J. Mater. Chem. B. 2 (2014) 295–304.

[44] M. Mazza, A. Patel, R. Pons, C. Bussy, K. Kostarelos, Peptide nanofibres as molecular transporters: from self-assembly to in vivo degradation, Faraday Discuss. 166 (2013) 181–194.

[45] A. Dehsorkhi, I.W. Hamley, J. Seitsonen, J. Ruokolainen, Tuning self-assembled nanostructures through enzymatic degradation of a peptide amphiphile, Langmuir. 29 (2013) 6665–6672.

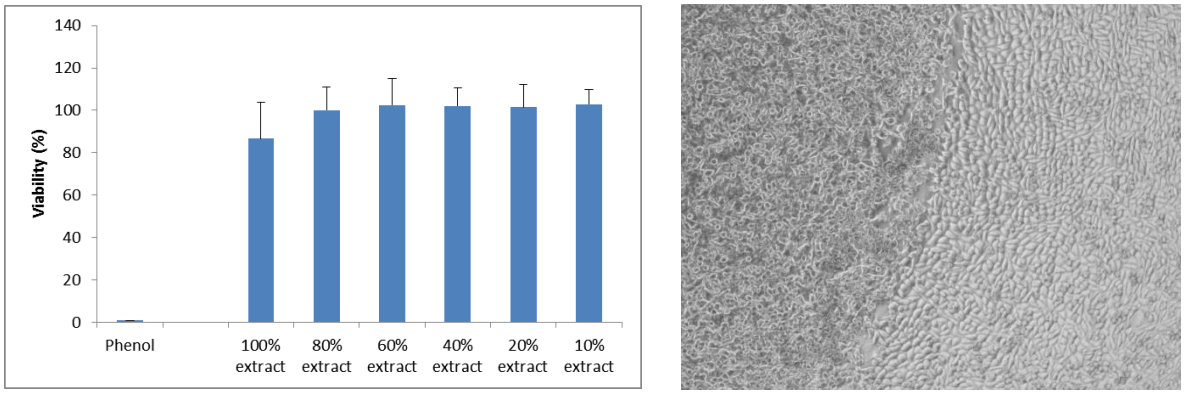

Figure 1.

Biocompatibility testing in accordance with ISO 10993-5. A) MTT assay- biocompatibility of P_{11}-4 extracts with L929 cells. B) Direct contact biocompatibility test shows L929 cells growing right up to the edges of the peptide. Arrows indicate L929 cells in direct contact with the peptide gel. There were no apparent adverse biocompatibility effects for P_{11}-4.

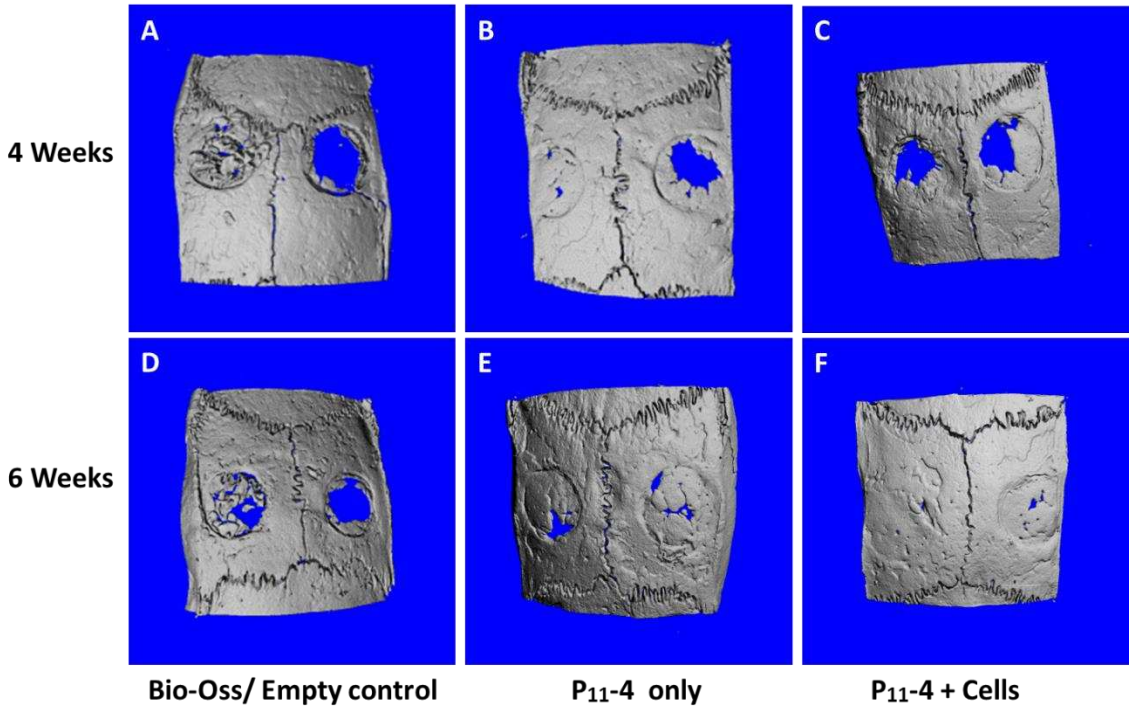

Figure 2.

Examples of qualitative microcomputer tomography (micro CT) reconstructed 3D images of 4 mm rat calvarial defects treated with A &D) Bio-Oss / Empty control , B & E) P_{11}-4 self-assembling peptide only , C & F) P_{11}-4 self-assembling peptide with cells. A single example is shown of sample defects from each treatment group and each time point.

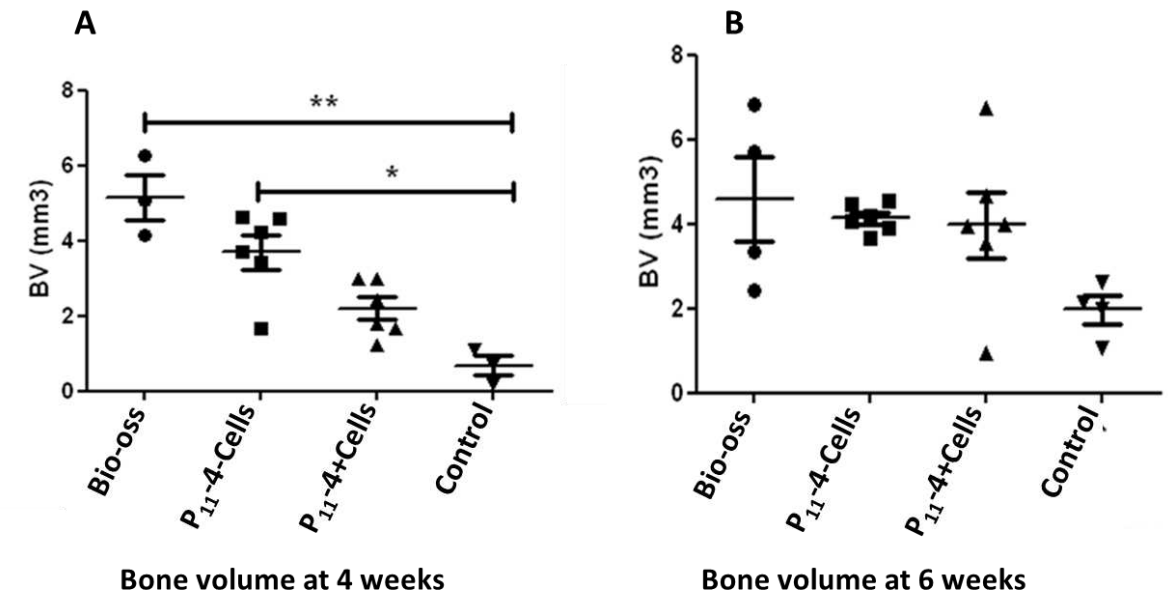

Figure 3.

Total new bone volume in calvaria defects based upon amount of mineralised tissue within the defects derived from micro-CT scans (please note that this will include Bio-Oss particles where present in the defect). Data analysed using Non Parametric test: Kruskal Wallis Test: Dunns post-test; Mean ± SEM : *$p<0.05$, **$p<0.01$.

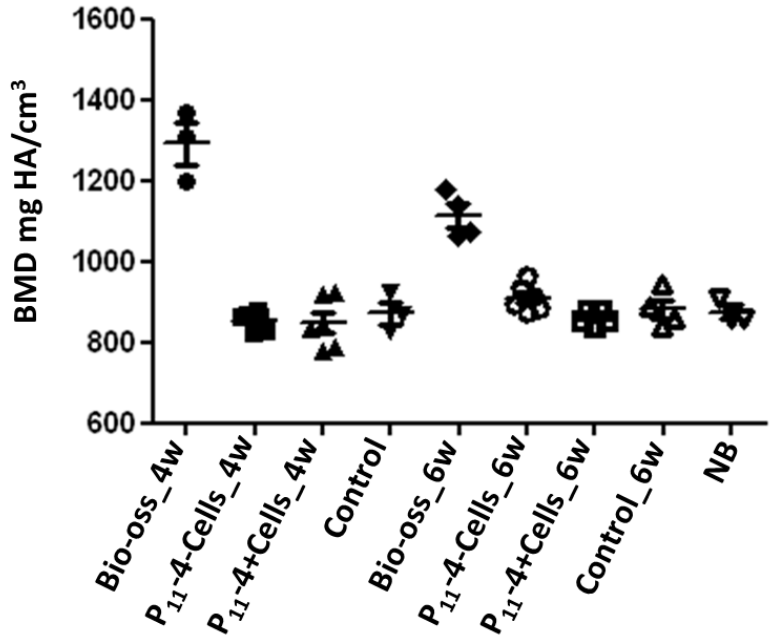

Figure 4.

Bone mineral density of new bone regenerated in calvaria defects at 4 weeks (4w) and 6 weeks (6w) based upon micro-CT data (please note that this will include Bio-Oss particles where present in the defect). Data analysed using Non-Parametric test: Kruskal Wallis Test: Dunns post-test; Mean ± SEM**.** NB: native old bone. No statistically significant differences were seen in bone density between bone formed within defects treated with P_{11}-4 self-assembling peptide with or without cells or between bone formed within the defects and adjacent native "old" bone.

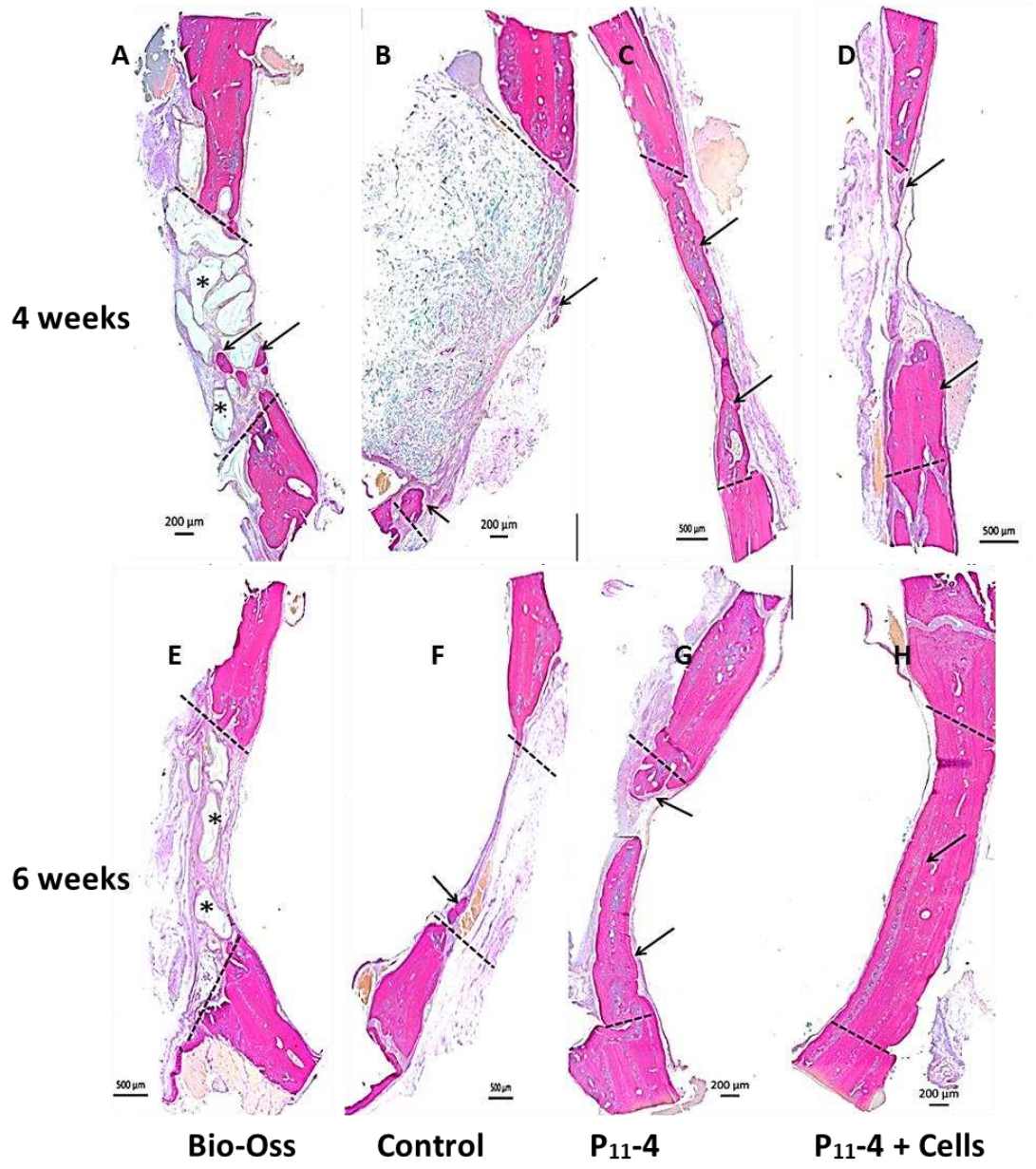

Figure 5.

Histological appearance of demineralised tissue in rat calvarial defects treated with Bio-Oss or P_{11}-4 self-assembling peptide with or without cells following staining with Van Gieson stain at 4 and 6 weeks post biomaterial implantation. Edges of the defects are demarcated with dotted black lines and new bone is indicated with arrows. A single example is shown for each treatment group and each time period. No obvious differences were seen in the

histological staining of the newly formed tissue in defects treated with P_{11}-4 self-assembling peptide with or without cells, or between newly formed bone and adjacent native "old" bone. Particles of Bio-Oss remaining in the defects are marked with *.

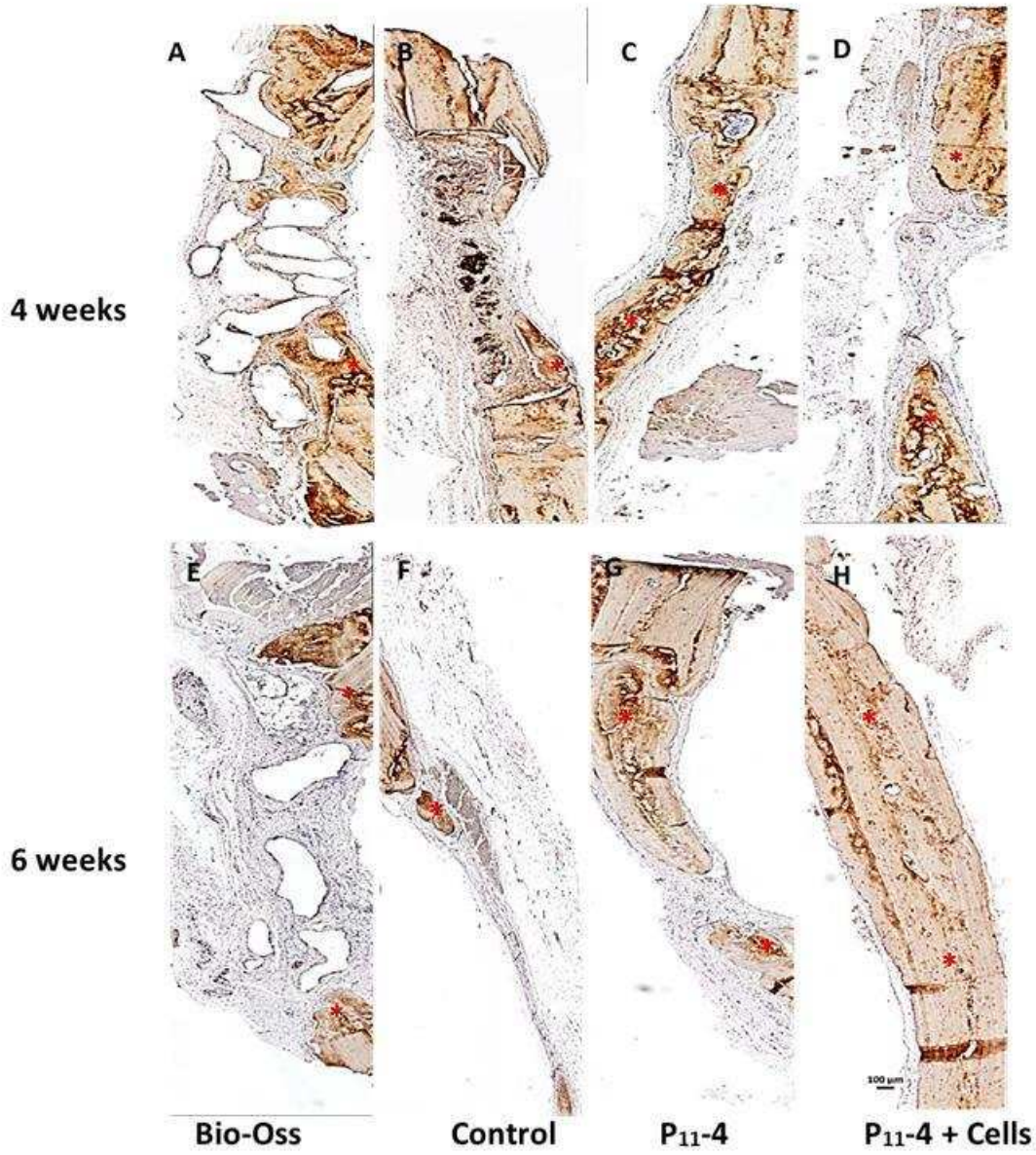

Figure 6.

Osteocalcin immunohistochemical staining at 4 and 6 weeks post biomaterial implantation in rat calvarial defects. Asterix indicates new bone formation that stains positively for osteocalcin.

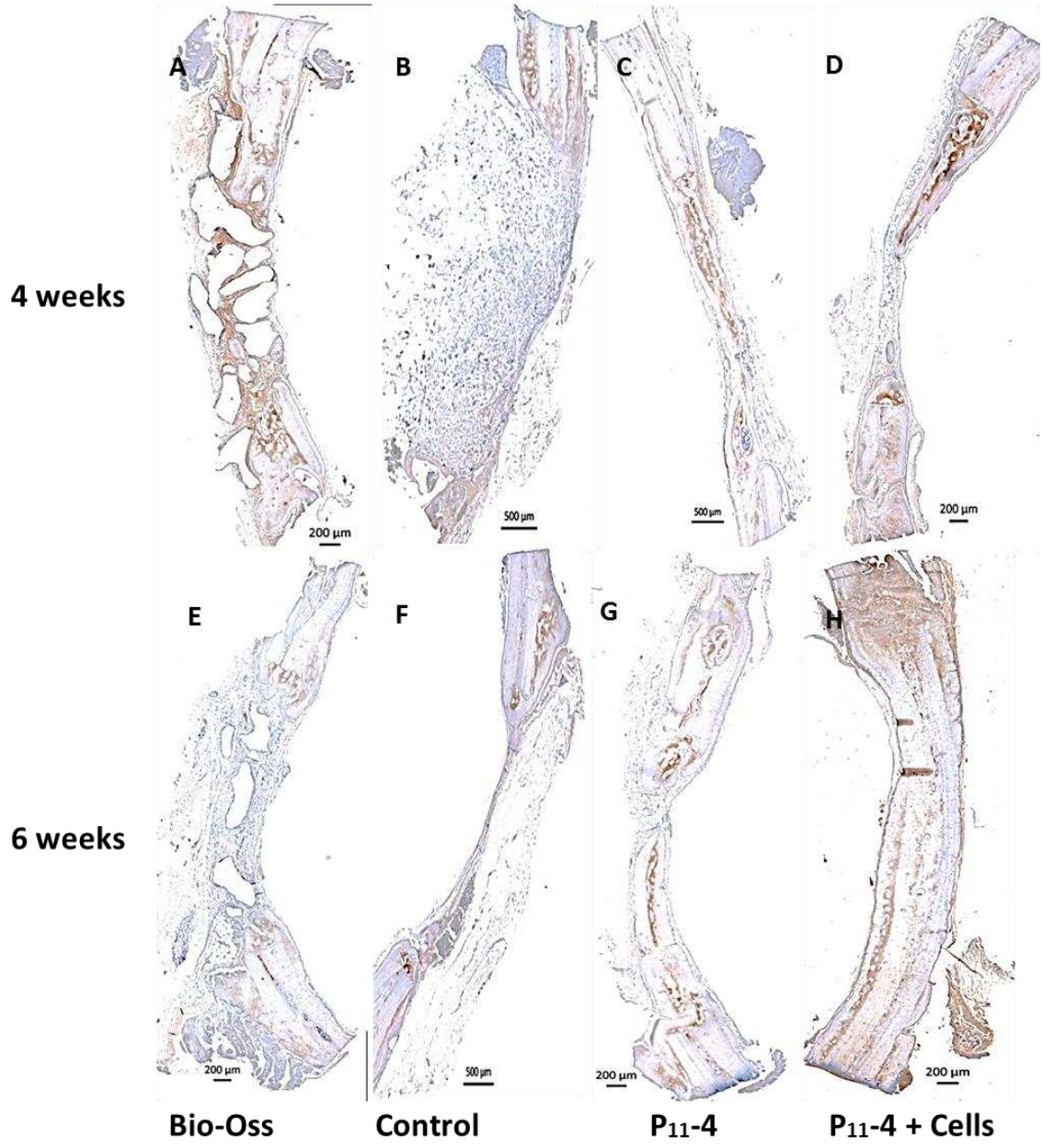

Figure 7.

Collagen type I immunohistochemical staining at 4 and 6 weeks post biomaterial implantation in rat calvarial defects.

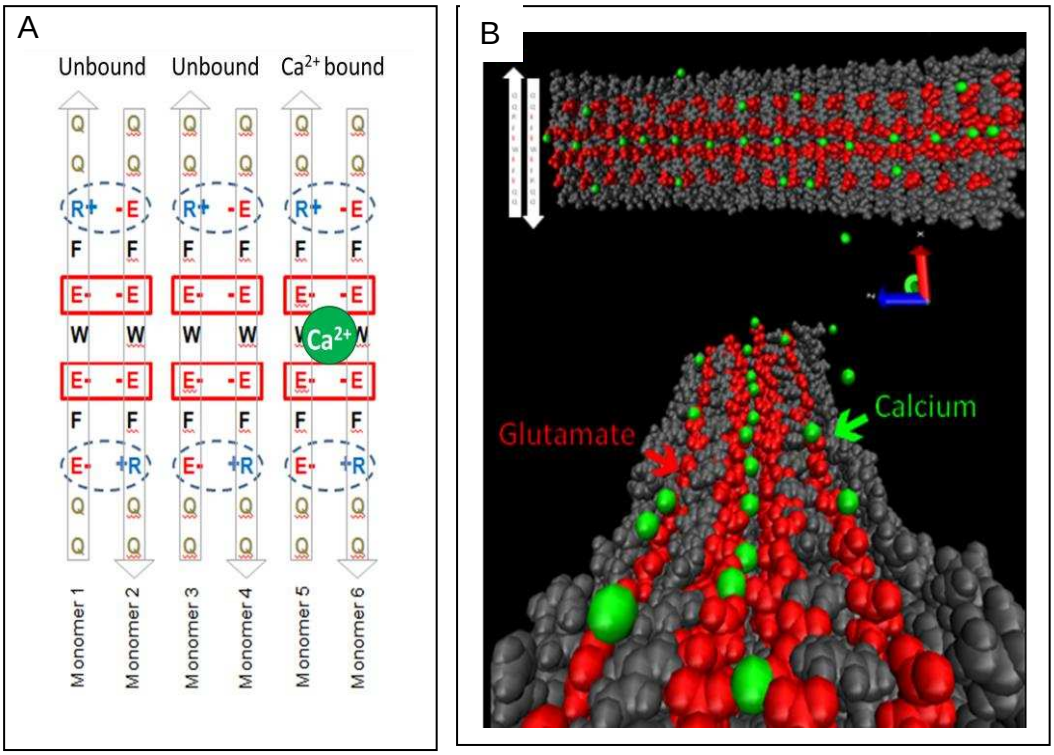

Figure 8.

In silico modelling using AMBER of association of assembled P_{11}-4 with calcium ions at pH 7.4. Amino acids in the P_{11}-4 primary sequence are shown via their single letter code. (A) Schematic showing anti-parallel alignment of 6 x P_{11}-4 monomers and preferred docking position of calcium (shown in green) between 4 adjacent glutamate (E) residues (boxed, shown in red). Dotted blue circles show predicted ionic interactions between adjacent glutamate (E) and arginine (R) residues. (b) Image showing predicted arrangement of P_{11}-4 ribbon in association with calcium ions (green). Top panel shows anti-parallel relationship of individual P_{11}-4 monomers (white arrows); bottom panel shows view along the assembled P_{11}-4 ribbon. Glutamic acid residues shown in red.

Sample	Total Number of defects evaluated at 4 weeks	Total Number of Defects evaluated at 6 weeks
Bio-Oss®	4	4
Empty Control Defect	4	4
P_{11}-4	6	6
P_{11}-4 with HDPSCs	6	6

Table 1: Experimental groups used in the in vivo study